

Peer Review File

Article Information: <https://dx.doi.org/10.21037/atm-22-4865>

Reviewer Comments

Comment 1: Please justify the use of FA in study in the Introduction Section.

Reply 1: Thanks for your advice. In the Introduction Section, we mainly explained the advantages of composite scaffolds in the field of tissue regeneration, as well as the application of our electrospun polycaprolactone/fluorapatite composite scaffold in previous research. The reason of incorporating FA nanoparticles into the ePCL scaffold has been discussed thoroughly in our previous research (Guo, T et al. Journal of Dental Research, 2014, 93(12): 1290-1295) and discussion (see Page 14 line 336 to page 15 line 367), so it is not repeated in detail in the Introduction Section.

Changes in the text: Hydroxyapatite (HA) and its composites, as common bioceramic materials, represent the most common form of bone mineral and provide mechanical strength and significant osteoinductive properties (34). However, because HA has a certain solubility in biological fluids and can be decomposed when heated, its long-term stability is poor (35). FA is a bioactive and biocompatible ceramic that is structurally and chemically similar to HA, and it presents high chemical stability. In addition, FA has much lower solubility in biological fluids than HA and presents excellent osteoinductive effects and antibacterial ability (36, 37). Our research group used FA crystals as a coating on the surface of ePCL nanofibers to optimize their surface microstructure and osteoinductive ability. According to SEM images (Fig. 2), the FA nanoparticles were uniformly distributed on the fiber surface and micropores in granular form in the ePCL/FA composite scaffolds, which is essential for the improvement of mechanical and biological properties of the scaffolds. As additional evidence for the presence of FA nanoparticle in ePCL/FA composite scaffolds, X-ray diffraction approach was employed. These distinct peaks in Figure 3A indicate introduction of crystalline properties into the amorphous nanostructure of the ePCL/FA

composite scaffolds due to the presence of FA and, therefore, indicate the formation of a biocomposite material. In addition, a series of in vitro experiments demonstrated that our ePCL/FA composite scaffolds have good biocompatibility and outstanding potential for osteoinduction and osteoconduction of dental pulp stem cells and human periodontal ligament cells (18, 20, 38). The hydrophilicity of the biomaterial plays an important role in bone tissue engineering by modulating osteogenic cell attachment, proliferation and differentiation for (39). As shown in Fig. 3B, we found that the ePCL/FA composite scaffolds improved hydrophilicity to overcome the inherent hydrophobicity of the pure ePCL polymer, which could be attributed to the increased surface area of the ePCL nanofibers owing to the existence of submicron structures on the surface in the presence of FA nanoparticles.

All studies demonstrated that incorporating FA nanoparticles into the ePCL scaffold improved the osteoinductive and osteoconductive properties as well as the wettability of the scaffold, which are insufficient in pure ePCL materials. Therefore, ePCL/FA composite scaffolds represent a biomaterial composite for possible application in bone tissue engineering.

Comment 2: There are no physicochemical analyzes showing that we are dealing with fluorapatite ceramics.

Reply 2: Sincerely thanks for your suggestion. We have supplemented the physicochemical analyzes of fluorapatite ceramics accordingly in the revised manuscript (see Page 7 line 152-155, page 11 line 248-255, and page 15 line 348-352 and Figure 3A).

Changes in the text: To evaluate the fluorapatite nanoparticle deposits on ePCL/FA composite scaffolds, X-ray diffraction (XRD) were performed. The Rigaku D/Max diffractometer was operated with a copper tube generated at a voltage of 40 kV and a current of 40 mA, set at a scan rate of 5°/min and 2 θ range of 10°-70°. X-ray diffraction, was employed to further characterize the physicochemical properties of ePCL/FA composite scaffolds, specifically the FA nanoparticle deposits. Figure 3A shows the XRD patterns of each group and the standard diffraction cards of pure FA samples

(JCPDS 15-0876). Compared with the FA standard diffraction card, it was found that the diffraction peak (shown in the red circle) was obvious with the change of synthesis time, which indicating that crystalline FA structures present in the composites (12, 18, 24h) as opposed to the completely amorphous nature of ePCL scaffolds. As additional evidence for the presence of FA nanoparticle in ePCL/FA composite scaffolds, X-ray diffraction approach was employed. These distinct peaks in Figure 3A indicate introduction of crystalline properties into the amorphous nanostructure of the ePCL/FA composite scaffolds due to the presence of FA and, therefore, indicate the formation of a biocomposite material.

Comment 3: Lines 216-220 – Statistical analysis. There are no info about post-hoc test used in the study.

Reply 3: Sincerely thanks for your suggestion. Our description of the statistical analysis of the study is not accurate. To be exact, we mainly determined statistical differences between bone mineral density (BMD), bone volume (BV), tissue volume (TV), BV/TV percentage, and water contact angle using a one-way analysis of variance, followed by Tukey's multiple comparisons test to compare individual groups. We accordingly have modified our manuscript (see Page 10, line 232-234).

Changes in the text: Statistical differences between experimental variants, including BMD, BV, TV BV/TV percentage and water contact angles, were determined using a one-way analysis of variance, followed by Tukey's multiple comparisons test to compare individual groups.

Comment 4: RESULTS SECTION. Too many comments in this section. Since the Authors decided to separate the chapters Results and Discussion, the comments (with references to the literature) in the Results Section are inappropriate.

Reply 4: Sincerely thanks for your reminders. We have removed all comment from the chapters Results to the chapters Discussion, and modified our text as advised (see Page 10, line 239 to page 11, line 269)

Changes in the text: As well known, that the design of scaffolds is a critical

consideration in bone tissue engineering. To observe the morphological structures of the electrospun PCL and ePCL/FA composite scaffolds, the samples were carefully studied via scanning electron microscopy. As shown in the SEM images (Fig. 2), each scaffold group had a micro/nanoscale topology. The surface of the ePCL nanofiber scaffolds was smooth and uniform, while the interior of the ePCL was arranged in a disordered manner to form an interwoven and porous three-dimensional network structure. The FA crystals were uniformly distributed on the fiber surface and micropores in granular form in the ePCL/FA composite scaffolds.

X-ray diffraction, was employed to further characterize the physicochemical properties of ePCL/FA composite scaffolds, specifically the FA nanoparticle deposits. Figure 3A shows the XRD patterns of each group and the standard diffraction cards of pure FA samples (JCPDS 15-0876). Compared with the FA standard diffraction card, it was found that the diffraction peak (shown in the red circle) was obvious with the change of synthesis time, which indicating that crystalline FA structures present in the composites (12, 18, 24h) as opposed to the completely amorphous nature of ePCL scaffolds.

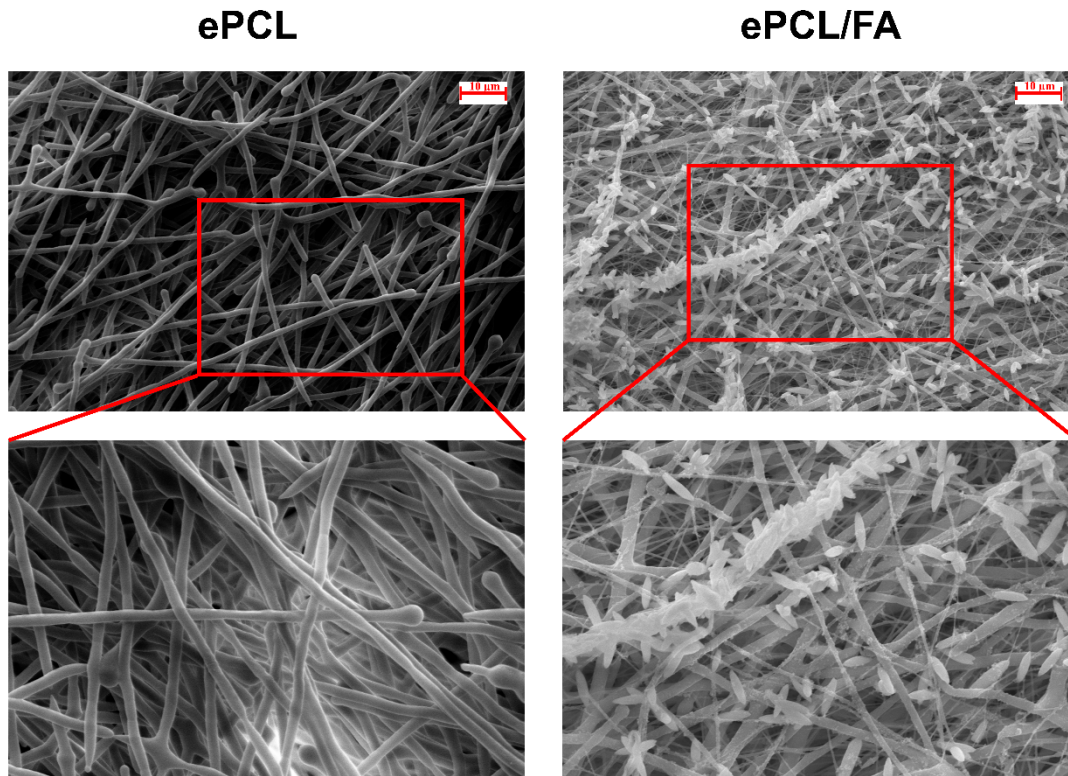
The surface hydrophilic properties of biomaterials influence the attachment and proliferation of different cells. The water contact angle of the material was measured to evaluate its wettability, with a contact angle below or above 90° indicating hydrophilicity and hydrophobicity, respectively. Fig. 3B summarizes the contact angle measurements performed on the pure ePCL and ePCL/FA composite scaffolds at different synthesis times (6, 12, 18 and 24 h). For the pure ePCL nanofibers, the average contact angle was greater than 100° . For the ePCL/FA group, the water contact angle was significantly decreased compared with that of the ePCL group ($p < 0.05$) and gradually decreased with an increase in synthesis time, indicating higher hydrophilicity.

Hence, these results indicated that PCL could be fabricated by electrospinning into a hydrophobic nanofibrous scaffold with a three-dimensional network structure similar to that of the extracellular matrix, and it could be modified by adding mineralization supplements, namely, FA crystals, to form an excellent hydrophilic biocomposite scaffold.

Comment 5: Figure 1A. Scale bars too small.

Reply 5: Thanks for the suggestion regarding scale bars. We have revised scale bars in the SEM images as suggested (Figure 2). Description was also added to the manuscript (see Page 23, line 585).

Changes in the text:



Comment 6: Figure 1B. The description of the figure lacks information on which statistical test was used.

Reply 6: Thanks for your thoughtful suggestion. We are very sorry for our negligence of the information on which statistical test was used. To clarify the issue, the related information has been added as following in the Statistical analysis section of revised manuscript (see Page 10, line 232-234).

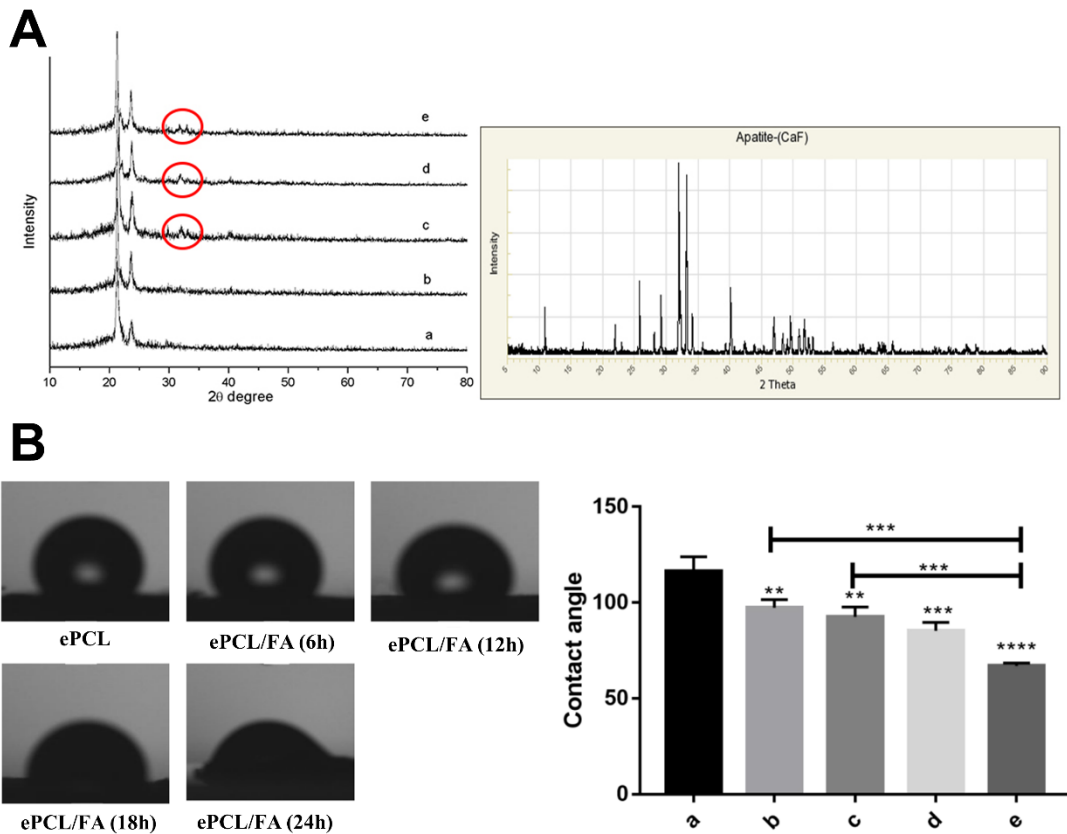
Changes in the text: Statistical differences between experimental variants, including BMD, BV, TV BV/TV percentage and water contact angles, were determined using a one-way analysis of variance, followed by Tukey's multiple comparisons test to

compare individual groups.

Comment 7: Figure 1B. Synthesis time points should be assigned to the appropriate images.

Reply 7: Thanks for your thoughtful suggestion. We have assigned the synthesis time point (6,12,18,24h) to the appropriate water contact angle images as suggested (see Page 23, line 588-592 and Figure 3B). As for the XRD patterns, the labels “a-e” indicate ePCL, ePCL /FA (6h), ePCL /FA (12h), ePCL /FA (18h), and ePCL /FA (24h), respectively. Considering that too long labels will cover the XRD patterns, we chose letter labels instead them and identified in figure legends.

Changes in the text:



Comment 8: Figure 2 should be rather placed in Methods Section.

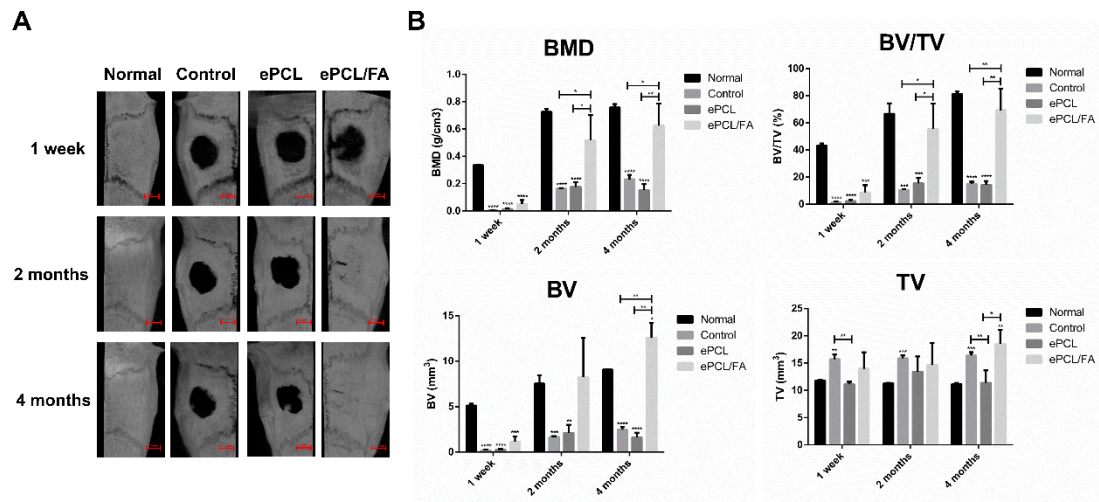
Reply 8: Thanks for your thoughtful suggestion. We have assigned the Schematic diagram (Figure 1) to Methods Section as suggested (see Page 9, line 200-204).

Changes in the text: After establishing the calvarial defect model, healing progressed uneventfully in all experimental animals and no postoperative complications were observed during the entire observation period. Schematic illustrations of the procedures for the construction and repair of calvarial defects in the SD rat model are shown in Figure 1.

Comment 9: Figure 3B. Charts are too small and subtitles barely visible.

Reply 9: Thanks for your thoughtful suggestion. We have readjusted the Figure 3B. Charts as suggested (see Page 24, line 599-604 and Figure 4B).

Changes in the text:

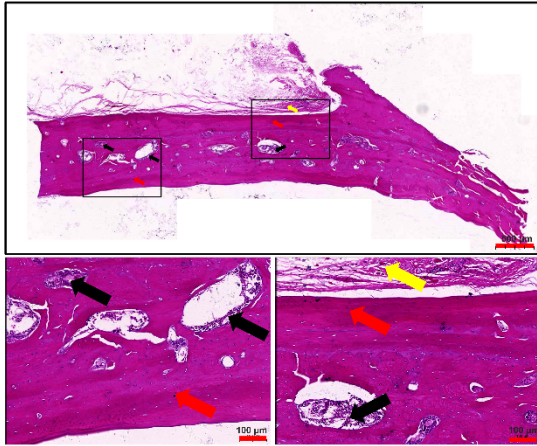


Comment 10: Figures 4-6. Scale bars too small.

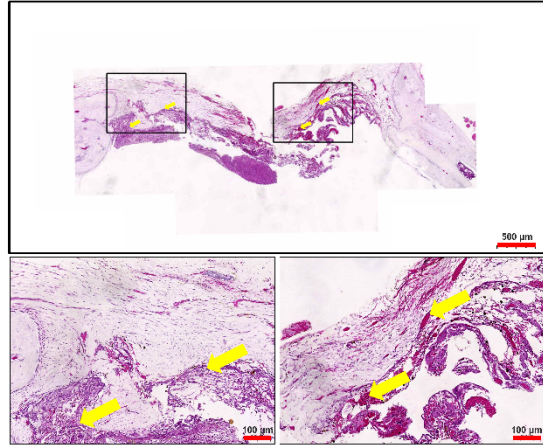
Reply 10: Thanks for the suggestion regarding scale bars. We have revised scale bars in the Figures 4-6 images as suggested (see Page 25, line 607 to page 27, line 621 and Figures 5-7).

Changes in the text:

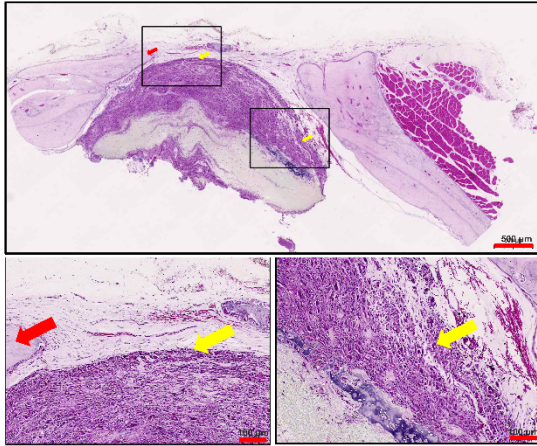
Normal



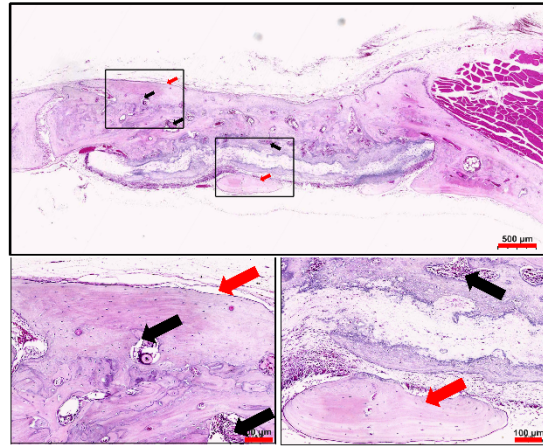
Control



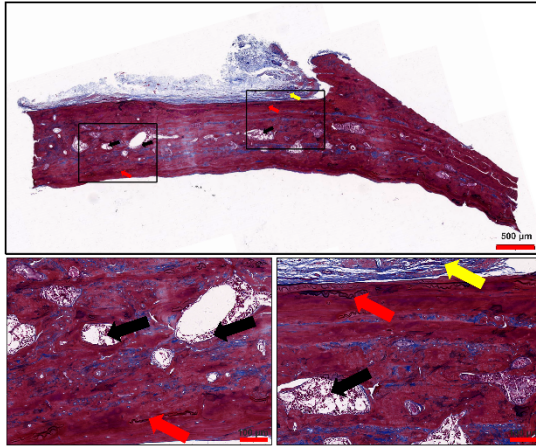
ePCL



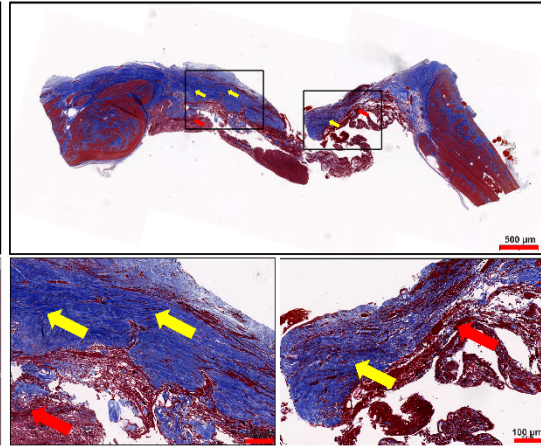
ePCL/FA



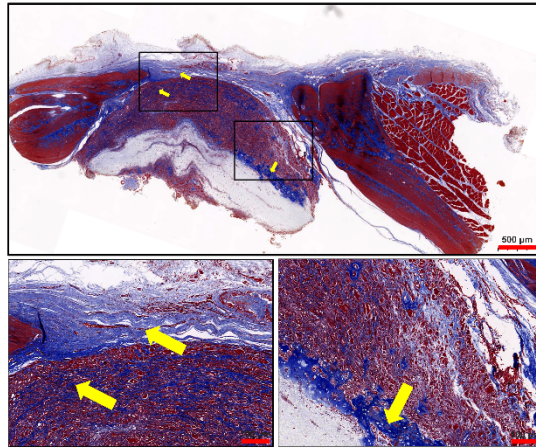
Normal



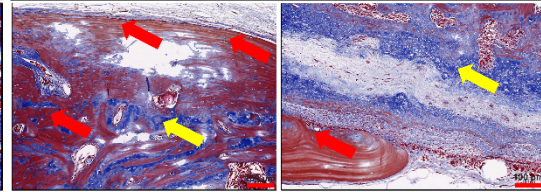
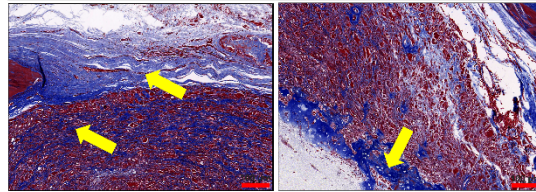
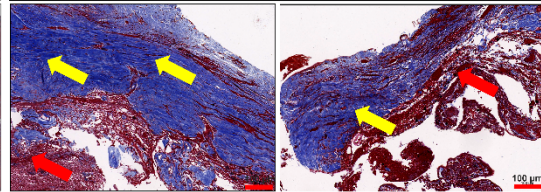
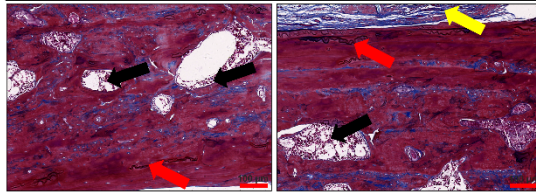
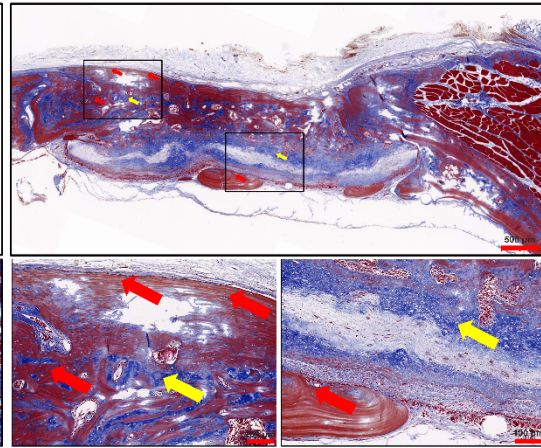
Control



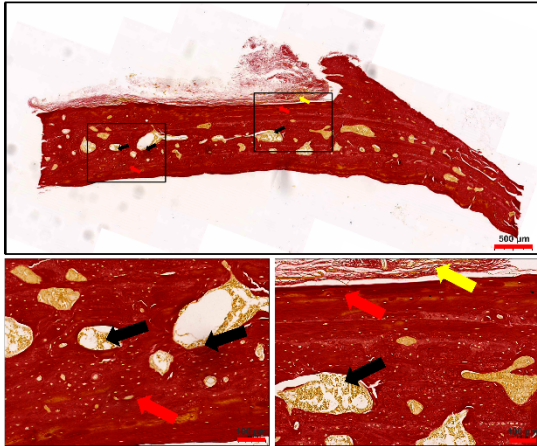
ePCL



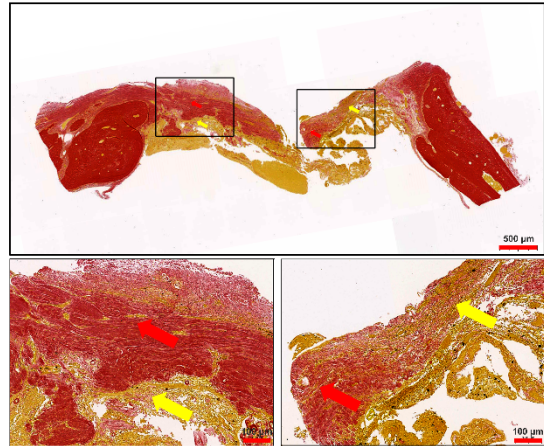
PCL + FA



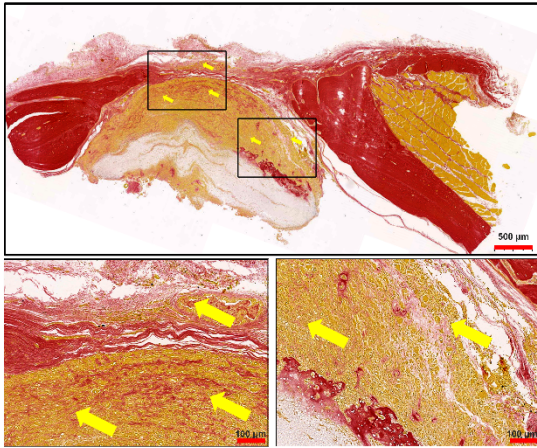
Normal



Control



PCL



PCL + FA

